Proceedings World Geothermal Congress 2023
Beijing, China, April 17 – 21, 2023

Characteristics of rock breaking with particle jet impact in deep geothermal reservoir

Jian Zhao [a,b*], Hualin Liao [b], Qicong Xu[c], Fulei Wan[c], Yiji Xu[b], Fengxia Shi[d]

[a] *Dongying Academy of Science and Technology, China University of Petroleum（East China）, Dongying 257061, China*

[b] *School of Petroleum Engineering, China University of Petroleum（East China）, Qingdao 266580, China*

[c] *Drilling and Production Engineering Technology Research Institute, CNPC Chuanqing Drilling Engineering Co. LTD, Deyang 618300, China*

[d] *College of Petroleum Engineering, Shandong Institute of Petroleum and Chemical Technology, Dongying, 257061, China*

* Corresponding author: Dr. Jian Zhao

E-mail: zhaojian-666@163.com

Abstract

Particle jet impact can fracture the rock, which can be utilized to improve the rock breaking efficiency of deep hot dry rock. In order to further explore the rock breaking characteristics, the breaking mechanism of hot dry rock under the action of particle jet impact were analyzed based on the Smoothed Particle Hydrodynamics (SPH) method, considering the deep geothermal high temperature and high confining pressure. The results show that the tensile stress generated by particle impact is much larger than the tensile strength of rock, and the rebound effect constituted an important factor in the crater diameter determination. Both the impact depth and breaking volume increased with the increase in the jet inlet velocity. Both the impact depth and breaking volume increases with the increase in the diameter. When the particle concentration exceeded a critical value (3%), both the impact depth and breaking volume increased slowly. The confining pressure will hinder the efficiency of particle impact rock breaking. High temperature will generate larger impact depth and breaking volume. The research can provide theoretical supports and parameter guidance for the application of efficient deep hot dry rock breaking technology with particle impact.

Keywords: Deep formation; Hot dry rock; Particle jet impact; Rock breaking efficiency; Rock breaking mechanism

1. Introduction

The particle jet is utilized in rock cutting [1,2] or in the shot blasting treatment technology [3,4] and is similar to the abrasive waterjet. However, spherical steel particles with a greater diameter (ranging from 0.5 to 5 mm) and lower particle concentration (ranging from 0.5 to 5% by volume) are utilized in the particle jet, which make it different from abrasive waterjet [5,6]. The steel particles act as an important factor in the erosion of rocks with a waterjet. The particles erupting from the nozzle at a high speed and frequency impact the rock within an extremely short time period and upon an extremely low sized contact area. The instantaneous contact stress is significantly high, thus changing the conventional rock breaking trend and significantly increasing the energy utilization [7,8].

The particle jet cutting performance is a nonlinear impact dynamics problem affected by various factors such as jet pressure, standoff distance, particle concentration, and the material. Moreover, the target material can be removed from the particle impact accelerated by water at a high velocity [9–11]. The solid particle erosion consists of the following two parts: deformation damage removal and cutting removal [12]. The rock is penetrated by particles with a high instantaneous dynamic load, high deformation, and short dwell time [13]. By the utilization of both the Newton motion equation and law of Meyer, the equation of the white iron crater volume penetration by particles was established, whereas the abrasive cut depth was proportional to the abrasive kinetic energy [14]. Experiments were also carried out for analyzing the effects of the cavity height on cavity erosion under a gas–solid flow. The spatial distribution of particles within the cavity and erosion related to particle

impacts for the variable cavity aft wall heights and for two particle sizes (44 and 106 μm) were studied. The maximum erosion rate was quite significant for higher sized particles [15]. A comprehensive modeling and computational study was presented for the erosion in elbows determination due to sand particles being entrained in air both by simulation and experimental methods, indicating that as the velocity increased, the metal loss increased following a power law [16].

With the objective of identifying and revealing the practical applications of a particle jet, investigation of the effects of the waterjet parameters on rock breaking performance is extremely important and highly desirable. The cutting depth efficiency tends to increase with increasing water pressure and traverse speed and with decreasing standoff distance. The cutting volume efficiency is strongly dependent on the standoff distance [17]. According to literature, with the contribution of the abrasive water jet, the drilling depth increased by ~63%, the thrust force and torque were reduced by ~15 and 20%, respectively, whereas the bit wear reduced significantly [18]. Both the theoretical analysis and experimental measurements demonstrated that the volume of the crater created by individual particle impingement, with the impingement velocity having been ranged between 5 and 11 m/s, was linearly proportional to the particle kinetic energy [19]. The kinetic energy of the wear particles that were removed increased linearly along with the erosion depth [20]. As the extent of strains exceeded the elastic limit, the impacted solid particles skidded over the surface. The threshold strain was theoretically derived as a function of the impact velocity and the rotating velocities as well as the particle surface contact duration [21]. A phenomenological model of the three-phased flow inside an abrasive waterjet machining cutting head was presented. The model was validated by an extensive set of experimental data with wide variations in cutting-head geometry, operating pressure, and abrasive mass flow rates [22]. An analytical model considering the size and shape of the abrasive particles was developed for the prediction of the brittle polycrystalline material total cut depth [23]. The tensile fracture caused by the shock pressure wave of abrasion was the main reason for the breaking of the rock [24,25]. A framework for sand collision modeling was presented including the effects of elastic, elastic–plastic and plastic deformations, surface adhesion, and size dependent property variations of sand [26]. The effects of pressure confinement on rock damage were analyzed by the ANSYS implicit–explicit solution [27]. The rock breaking caused by particle impact was investigated by the one-dimensional stress wave theory [28]. The abrasive wear is a rapid and severe process due to the contact between the abrasives and the solid material surfaces. This type of wear is usually classified into the following two categories: (i) the 2-body abrasive wear and (ii) the 3-body abrasive wear [29]. An integral approach with consideration of both the plastic and elastic–plastic material removal modes was presented. The erosion was characterized by two failure modes, the intercrystalline fracture and lateral cracking, whereas the power exponent regarding the particle velocity effects was 2.44 [30,31].

The smoothed particle hydrodynamics (SPH) simulations were utilized for particle embedment simulation. Regarding a given particle size, the embedment increased along with the incident velocity, whereas a critical minimum velocity, below which embedment would not occur, was predicted [32]. An SPH simulation of a cone penetrometer test in soft, cohesive soil was implemented. The higher soil strengths could be reproduced in the simulation if an improved shear model including the non-negligible friction angle was provided [33]. The energy absorption behavior of empty and aluminum metal foam-filled tubes with various taper angles was evaluated by the Finite Element Method (FEM) coupled with SPH [34]. A coupled FEM/SPH modeling technique was investigated for the numerical simulation of the quasi-static axial crushing of polystyrene foam-filled aluminum thin-walled aluminum tubes [35]. An FE methodology was developed for tensile stresses in the coating surface under a single particle impact analysis simulating the particulate erosion conditions [36].

Besides, most previous studies focused on rock cutting with the pure waterjet or abrasive waterjet, and not the particle jet, being different in utilization of spherical steel particles with a higher diameter and lower particle concentration. In a typical abrasive waterjet, the shape of the abrasives is irregular, and a garnet or quartz is usually utilized as the abrasive with diameter ranging from 0.06 to 0.3 mm. These characteristics of the abrasives

lead to the serious wearing of the parts (such as nozzles and pipes) of an abrasive waterjet. In contrast, during a particle jet, the equipment wears only slightly. In most previous studies, the effects of waterjet were not considered, and the FEM/SPH method was rarely utilized for the investigation of the particle jet rock breaking problems. This technology can significantly enhance the hot dry rock breaking efficiency owing to the higher kinetic energy of particles. In practice, a multi large spherical steel particle impact is required for the rapid cutting of the rock. Furthermore, in most previous studies only the theoretical calculation or the experimental method was utilized for the investigation of the rock breaking performance, and the effects of high confining pressure and temperature were seldom studied.

In this study, a numerical simulation was utilized for the establishment of the relationship between the rock breaking performance and particle parameters for hot dry rock, with consideration of the effects of waterjet based on the SPH method, conforming to practical operational conditions in an effort for providing an efficient design for practical application.

2. Finite element model

2.1. Smoothed Particle Hydrodynamics-Finite Element Method

In the SPH method, the continuous fluid is dispersed to interact with particles, and the change in particles is utilized to describe the change in the continuous fluid by the Diffuse Element Method. The SPH method is widely utilized in the high deformation of penetration study [32–35]. In this study, the SPH coupled with the FEM was applied to investigate the relationship between the particle jet parameters and the rock breaking performance (depth and volume). Furthermore, both the SPH and FE methods were utilized for the particle jet and rock models establishment, respectively.

Both the particle and water were modeled by the SPH method, which was a pure Lagrange method and did not require a mesh based upon the interpolation theory. A series of uniformly distributed smoothed particles was utilized having a variety of physical properties for the partial differential equations solution under various conditions. The kernel estimated value *f*(*x*) could be expressed by using Eq. (1) [36–39] as follows:

$$f(x)=\int_{\Omega} f(x')W(x-x',h)dx' \tag{1}$$

where $f(x)$ is the function of the 3D coordinate vector *x*, Ω is the support domain of the point *x*, $x-x'$ is the distance between the particles, *h* is the smooth length of the SPH particle changing along with time and space, and $W(x-x',h)$ is the kernel function, usually defined by the auxiliary function ($\theta(x-x')$):

$$W(x-x',h)=\frac{1}{h(x-x')^{d}}\theta(x-x') \tag{2}$$

where *d* is the space dimensionality.

The cubic b spline curve is most commonly utilized for a smooth function in the SPH method as described by the following equation:

$$\theta(u)=C_{\mathrm{b}}*\begin{cases}1-\frac{3}{2}u^{2}+\frac{3}{4}u^{3}, |u|\le 1\\ \frac{1}{4}(2-u)^{3}, 1\le u\le 2\\ 0, |u|\ge 2\end{cases} \tag{3}$$

where C_b is the normalization constant, confirmed by the space dimension $u = \frac{x - x'}{h}$.

Substitution of Eq. (2) into Eq. (1) and the conversion of the continuous form integral equation into the discrete form equation led to the following equation:

$$f(x) = \sum_{i=1}^{n} \frac{m_i}{\rho_i} \frac{1}{h(x - x_i')^d} \theta(x - x_i') \tag{4}$$

where ρ_i is the density of particle *i* and m_i is the mass of particle *i*.

2.2. Water and Rock Damage Model

The 1# elastic material model in the ANSYS-DYNA was utilized for particles, and the parameters are listed in Table 1 [37,38].

Table 1

1# elastic material model parameters for particles [37,38]

Material	ρ_p [g/cm^3]	υ_p	E_p [GPa]
Particle	7800	0.3	210

The MAT_NULL material model was utilized for water. The GRUNEISEN state equation expressed by Eq. (5) was also utilized for water and the parameters are also listed in Table 2 [40–43]:

$$P_{MG} = \frac{\rho_0 C_{MG}^2 \left[1 + \left(1 - \frac{\gamma_0}{2}\right)\mu - \frac{a}{2}\mu^2\right]}{\left[1 - (S_1 - 1)\mu - S_2 \frac{\mu^2}{\mu + 1} - S_3 \frac{\mu^3}{(\mu + 1)^2}\right]} + (\gamma_0 + a\mu)Ea \tag{5}$$

where P_{MG} is the pressure, *E* is the internal energy per unit volume, C_{MG} is the intercept of the u_s - u_p curve, ρ_0 is the density, S_1, S_2, and S_3 are the slope coefficients of the curve, γ_0 is the GRUNEISEN constant, and *a* is the volume correction.

Table 2

Water parameters for simulation [43]

Material	ρ_0 [g/cm^3]	C [m/s]	S_1	S_2	S_3	a	γ_0
Water	1	1480	2.56	-1.986	0.2286	1.397	0.49

The Holmquist Johnson Cook (HJC) model was utilized for the rock, which is usually employed as the rock damage model under a high deformation, high strain rate, and high pressure, with consideration of the effects of rock material damage, strain rate, and hydrostatic pressure to the yield force [44,45]. The yield surface equation of the HJC model is as follows:

$$\sigma^* = [A(1 - D) + BP^{*N}](1 + C\ln \dot{\varepsilon}^*) \tag{6}$$

where σ^* is the equivalent stress which is dimensionless and obtained from the actual equivalent stress divided by the static compressive strength f_C', P^* is the hydrostatic pressure which is dimensionless and obtained from the actual hydrostatic pressure divided by the static compressive strength f_C', and $\dot{\varepsilon}^*$ is the strain rate that is

dimensionless and obtained from the actual strain rate divided by the reference strain rate $\dot{\varepsilon}_0$. *D* is the damage ratio and *A*, *B*, *N*, and *C* are the material strength parameters.

The damage was described by the accumulation of the equivalent plastic and plastic volumetric strains. The damage evolution equation is represented by Eq. (7) [46,47]:

$$D = \sum \frac{\Delta\varepsilon_p + \Delta\mu_p}{\varepsilon_p^f + \mu_p^f} \tag{7}$$

where $\Delta\varepsilon_p$ and $\Delta\mu_p$ are the equivalent plastic and plastic volumetric strains, respectively, in an iteration, and ε_p^f and μ_p^f are the equivalent plastic strain and plastic volumetric strain, respectively, under the atmospheric pressure. The parameters of the HJC model for the rock during the simulation are listed in Table 3 [46].

Table 3

HJC model parameters for the rock during simulation [46]

ρ [kg/m^3]	*G* [GPa]	$f_C^{'}$ [MPa]	*A*	*B*	*C*	*N*	S_{MAX}	D_1	D_2
2600	20.8	61	0.93	1.60	0.08	0.79	7.0	0.04	1.0
ε_{fmin}	*T* [MPa]	p_c [MPa]	μ_c	p_1 [GPa]	μ_1	k_1 [MPa]	k_2 [MPa]	k_3 [MPa]	$\dot{\varepsilon}_0$
0.004	4	2.03	0.66	1.0	0.072	85	-171	208	1

2.3. Finite element model

The 3D FE model established for a particle jet is presented in Fig. 1. The grid number of the rock utilized in this case was approximately 180,000. The SOLID 164 element with 8 nodes was applied for rock meshing. The number of SPH particles for the steel particles was proportional to the SPH particles for water that could be determined by the designed particle concentration (the particles concentration is 1% by volume in Fig. 1). The NON-REFLECTING boundary condition was utilized to constrain the underside and the four side faces of the rock. The contact type to the rock was set as *CONTACT_ERODING_NODES_TO_SURFACE. The inlet velocities of both water and particles were set as the initial velocities. In particular, the red color in the waterjet was utilized to represent the spherical steel particles as shown in Fig.1. The rock erosion was resulted by the removal of the rock elements. When the equivalent plastic strain exceeded the ε_{fmin} = 0.004 (the minimum equivalent plastic strain that caused the rock to become broken as listed in Table 3), the FE of the rock began to be removed.

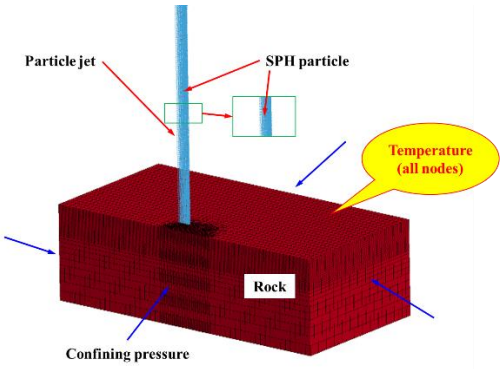

Fig. 1. 3D Finite element model for the particle jet based on the SPH–FEM method.

Confining pressure appling steps are as follows: Define the load curve by keyword *Define_Curve; Set the "Segment" set on the plane where confining pressure is required; Load curve is applied to the "Segment" set by keyword *Load_Segment_Set; Define *Interface_Springback_Lsdyna keyword. Select all the nodes and apply the temperature loads to hot dry rock by keyword *Initial_Temperature_node, and solve and output *K file.

2.4. Particle jet parameters

The rock breaking simulation were performed under various particle jet parameters (particle velocity, particle diameter, concentration, confining pressure, and temperature). The particle velocity was controlled from 100 to 240m/s. The particle diameter ranged from 0.5 to 2.5 mm, whereas the particle concentration within the waterjet was changed from 0.5 to 5% by volume. The confining pressure ranged from 0 to 50 MPa. The temperature for the hot dry rock varied from 100 to 400℃. The simulation parameters for the particle jet impact are listed in Table 4.

Table 4

Particle jet parameters

Water pressure (P_w) [m/s]	100	136	165	195	220	240
Particle diameter (d_p) [mm]	0.5	1	1.5	2	2.5	
Particle concentration by volume (C_p) [%]	0.5	1	2	3	4	5
Confining pressure (P_c) [MPa]	0	10	20	30	40	50
Temperature (T_i) [℃]	25	100	200	300	400	

3. Result and discussion

The rock breaking mechanism and effects particle jet parameters on the rock breaking depth and volume were analyzed by numerical simulation.

3.1. Analysis of rock breaking process

The rock breaking by particle jet impact is presented in Fig. 2. The particles with a high velocity were accelerated by the fluid impact upon the rock surface. At a higher erosion depth, the volume of the crater was higher along with the continuous impact of particles. Particles following impact constantly rebounded and left the crater area as presented in Fig. 2. The diameter of the initial formed crater was almost the same as the jet diameter as presented in Fig. 2b. Because the particle diameter was higher, the particle density was higher than the density of ordinary abrasives and the rock was hard to be penetrated, the particles impacted the hard rock and rebounded. Moreover, as well-known, the secondary flow of the fluid carrying particles outside the primary impact zone can intensify this rebound effect. When the dwell time increased, the rebound particles continuously stroke the side face of the craters and the diameter of the craters increased due to the rebound effect as presented in Figs. 2c and d. Therefore, the rebound effect acted as an important factor in the crater diameter determination during the particle jet impact.

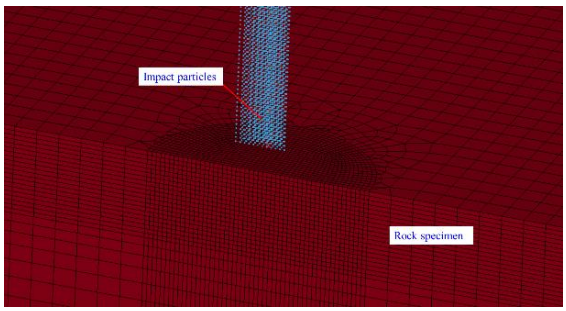

(a) t = 0 s

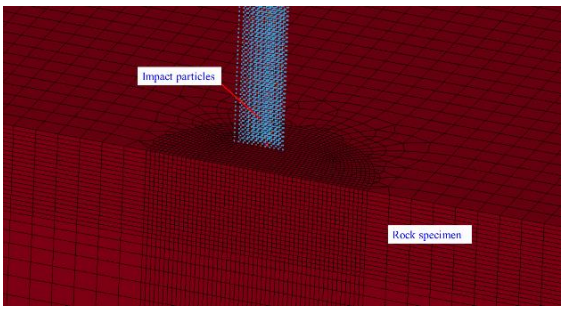

(b) t =0.04s

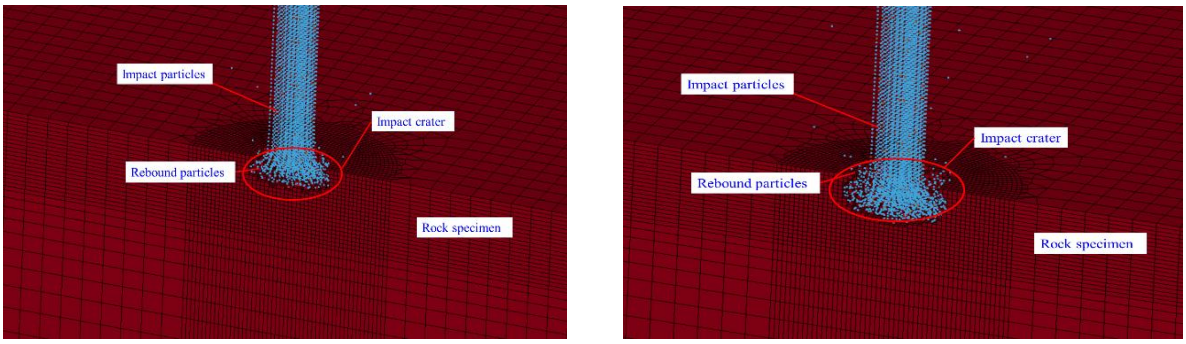

(c) t = 0.08s (d) t = 0.12s

Fig. 2. Rock breaking process by particle jet

For brittle materials such as concrete, rocks, and cast iron, the First Strength Theory (or the Tensile Strength Theory) is usually utilized to estimate whether these materials are broken or not. The value of the first strength theory was also the 1st principal stress (maximum principal stress) in the ANSYS software. During impact, the 1st principal stress distribution of the rock is presented in Fig. 3. The rock began to break when the 1st principal stress exceeded the tensile strength of the rock. The maximum value of 1st principal stress was 23.1 MPa, significantly higher than the tensile strength of the rock (the tensile strengthen of marble was ~4 MPa) in the time range of 0.04 s; therefore, the rock could be broken easily (Fig. 3b). The higher values of the 1st principal stress were distributed on the surface areas of the crater and the 1st principal stress became lower when the distance between the points of the rock and the surface of the crater increased as presented in Figs. 3 b–d. The bottom of the crater, where the 1st principal stress was higher, was the main broken area of the rock. The 1st principal stress was higher only in the side of the crater where the rebounding particles impacted, as presented in Figs. 3c and d. The side of the rock could not be broken because of this rebound impact and this result was well consistent with the results presented in Fig. 2.

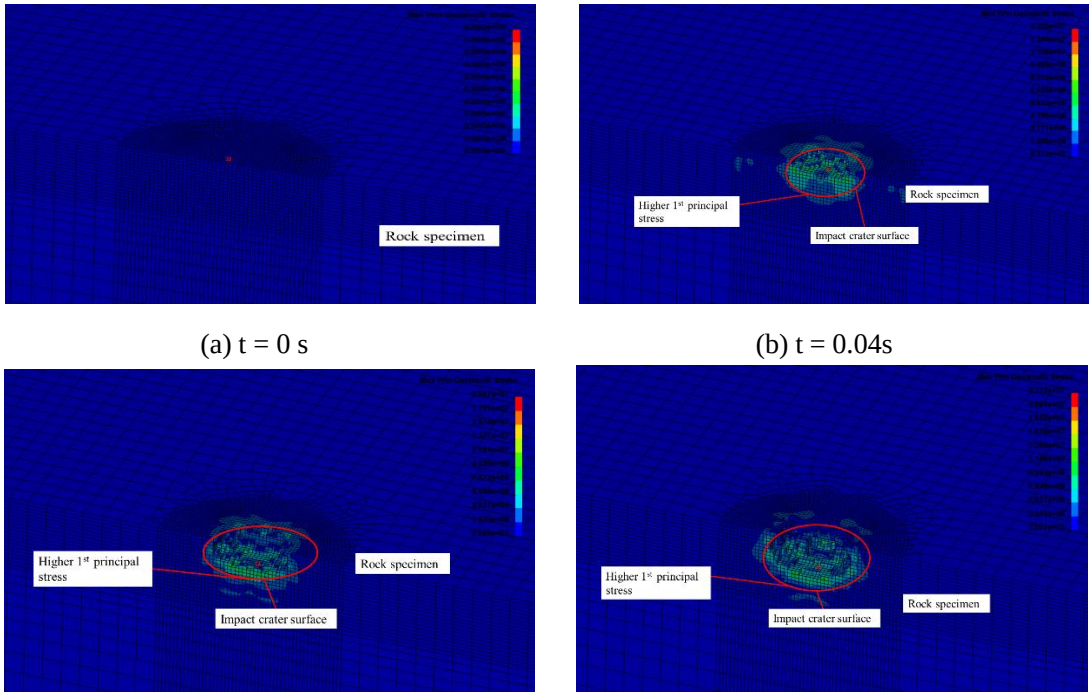

(a) t = 0 s (b) t = 0.04s

(c) t = 0.08 s (d) t = 0.12 s

Fig. 3. The 1st principal stress distribution.

3.2. Effects of particle jet parameters

3.2.1. Jet inlet velocity

The particle jet energy is directly related to the jet inlet velocity (v_w). Therefore, the impact depth and breaking volume of the rock increased as the jet inlet velocity increased in agreement with previous findings [9,48]. Fig. 4 demonstrates the effects of jet inlet velocity on the impact depth and volume. The results clearly indicated that the impact depth increased as the v_w increased. The impact depth and velocity had an approximately linear relationship. The depth of cut increased rapidly with the increase in the kinetic energy of the impacting particles due to the increase in the water inlet velocity [48,49]. As the velocity increased, the breaking volume increased. When the velocity increased, both the kinetic energy of the particles and water would increase significantly, leading to a higher impact energy that acted on the rock, consequently the rock could easily be broken. Therefore, the rock breaking volume increased at a higher water inlet velocity. Besides, due to the higher density of particles and harder rock, it was believed that the energy increase of particles was the main factor that influenced the rock breaking volume changes.

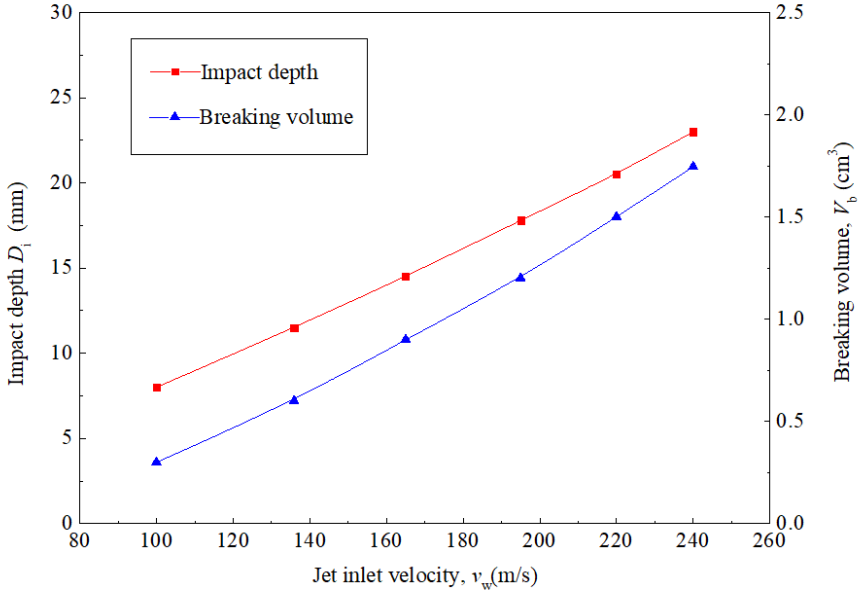

Fig. 4. Velocity effect on impact depth and volume.

3.2.2. Particle Diameter

The particle diameter (d_p) is an important parameter that is directly related to the particle kinetic energy. Particles with a higher diameter can generate a higher energy that impacts the rock. Fig. 5 exhibits that the impact depth increases with the increase in the diameter, and this result is in agreement with previous findings [50–53]. Furthermore the results indicated a nearly linear relationship between the impact depth and particle diameter. This could be explained by the fact that lower sized particles had a lower kinetic energy compared to higher sized particles due to lower masses. Therefore for a single particle, a higher sized particle could cause a higher impact force that would act on the rock due to the higher kinetic energy than lower sized particles. Moreover, lower sized particles were diverged further from the nozzle axis to the exterior and hit on a higher sized region on the rock surface, whereas higher sized particles changed only slightly the corresponding trajectories and hit on a lower sized region encircling the nozzle axis. Consequently, regarding the same particle flow rate, the higher sized particles might cause a high impact concentration (the number of repeated impacts upon the same location) because the impact area was lower sized [52]. The breaking volume increases with the increase in the diameter. When the particle diameter exceeded 1.0 mm, the breaking volume began to increase rapidly due to the higher kinetic energy and higher impact concentration for higher sized particles. Furthermore, the speed increased as the particle diameter increased (the slope of the curve increased as the particle diameter increased. Therefore, the breaking volume of a particle water jet strongly depends on particle diameter.

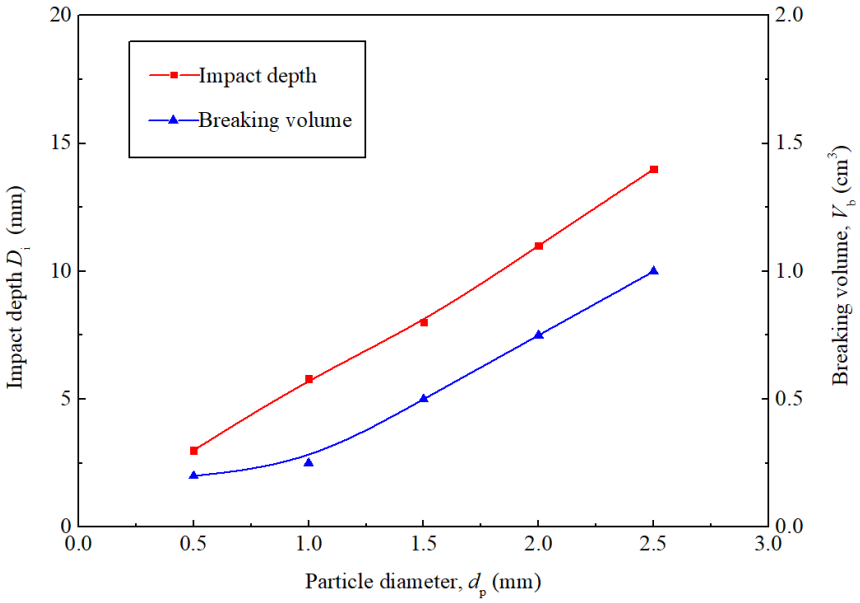

Fig. 5. Diameter effect on the impact depth and volume.

3.2.3. Particle Concentration

The particle concentration (C_p) is defined as the volume concentration of the water flow. The results as presented in Fig. 6 indicate that the impact depth increases as the particle concentration increases. When the particle concentration was below the critical concentration (3%), the impact depth increased rapidly with the increase in the concentration. Besides, when the particle concentration was >3%, the impact depth increased slowly. This could be explained by the fact that an interference effect caused by the collisions between the incident and rebound particles existed, which was studied in detail [54–57] as presented in Fig. 7. Furthermore it was quite useful for the critical concentration or mass flow to be estimated for interference effects minimization during rock breaking, in order for a higher proportion of the stream energy leaving the nozzles to reach the intended target. It could be confirmed that the critical concentration was 3% in this study. When the particle concentration was <3%, the probability of collisions was low, and most particles arrived at the target surface without sustaining an inter-particle collision, therefore the impact depth increased dramatically. When the particle concentration was >3%, the percentage of particles without collision reduced dramatically, possibly resulting in the significant decrease in the particle kinetic energy eroding the target, therefore the impact depth increased slowly. Moreover, as the incident angle was higher (α = 90°), the collision zone size was higher, and therefore the probability of survival was quite lower than that at a lower incident angle [55]. The interference effect was quite complicated; therefore, the degree of particle–particle interactions will be investigated in the future. The breaking volume also increases with the increase in the particle concentration, similar to the effects of concentration on the impact depth. When the particle concentration was below the critical concentration (3%), the breaking volume increased rapidly with the increase in the concentration. Besides, when the particle concentration was >3%, the breaking volume increased slowly owing to interference caused by the collisions between the incident and rebound particles.

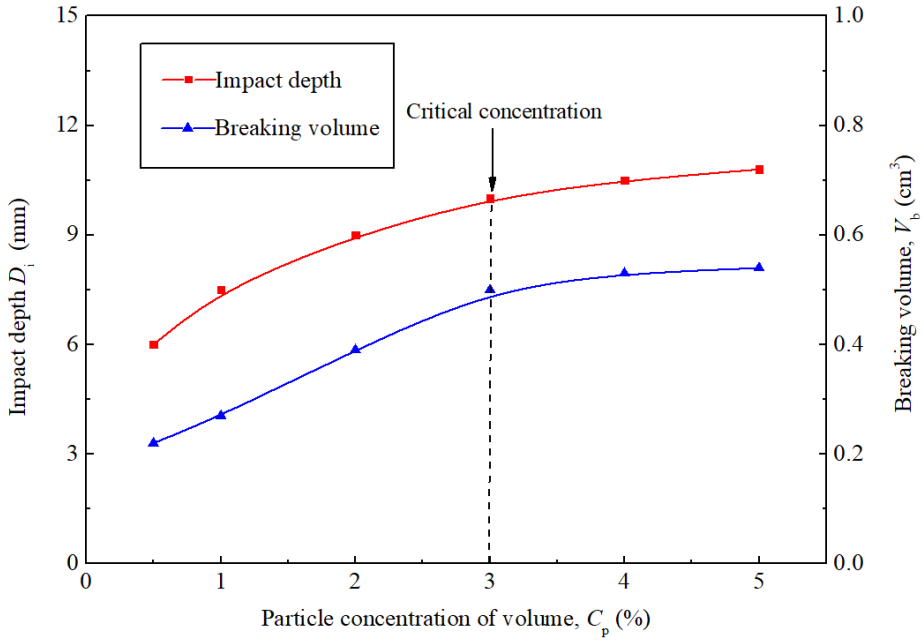

Fig. 6. Concentration effect on the impact depth and volume.

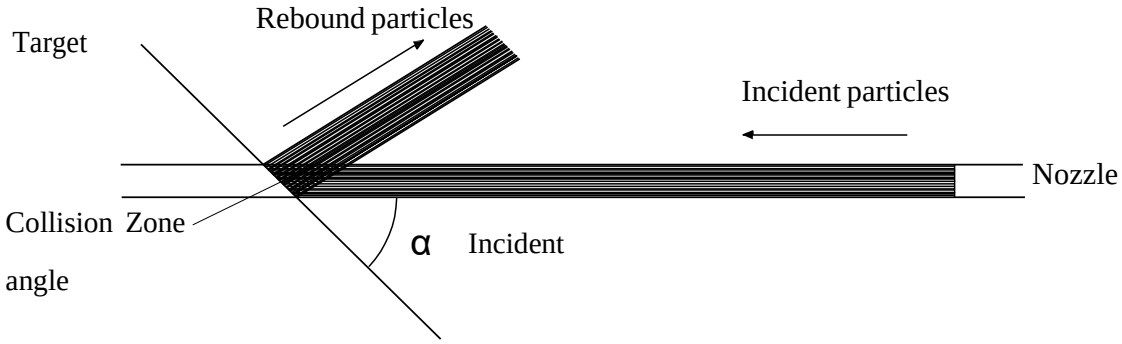

Fig.14. Schematic diagram of collisions between incident and rebound particles [53].

3.2.4. Confining Pressure

The relationship between the impact depth and breaking volume and the standoff distance for various confining pressure is presented in Fig. 7. With the increase of confining pressure, the impact depth and breaking volume decrease. When the high pressure particle jet contacts the rock, the energy is exchanged rapidly, and the particle impact produces huge impact force on the rock surface. When the strength of tensile and shear strength of the rock is exceeded, the rock is broken. Because the tensile strength of the rock will be improved correspondingly under high confining pressure, the damage development of the rock is slow under high confining pressure. In addition, part of the energy of particle impact will propagate in the rock in the form of stress waves, resulting in tensile effect on the rock. High confining pressure will affect the peak value and frequency of stress waves in the rock, thus weakening the damage effect of stress waves on the rock. The rock damage and breakage time required will increase. Therefore, with the increase of confining pressure, the impact depth and breaking volume decrease.

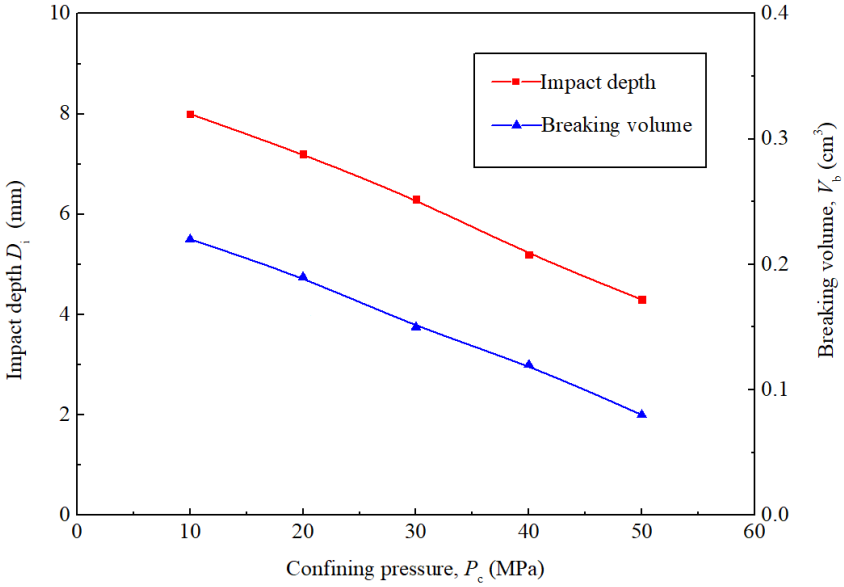

Fig. 7. Confining pressure effect on the impact depth and depth

3.2.5. Temperature

The relationship between the impact depth and breaking volume and the standoff distance for various temperature is presented in Fig. 8. With the increase of temperature, the impact depth and the breaking volume increase. For hard and brittle rocks, uniaxial compressive strength and fracture toughness decrease obviously with the increase of temperature [58]. As the temperature of the rock increases, the impact of high-speed particles on the rock surface produces huge impact stress. Due to the reduction of the strength of the rock, the particle impact is more likely to produce tensile shear failure inside the rock, which is more conducive to the generation, expansion and extension of cracks inside the rock. Therefore, with the increase of the temperature, the impact depth of the rock and the volume of broken rock constantly increase.

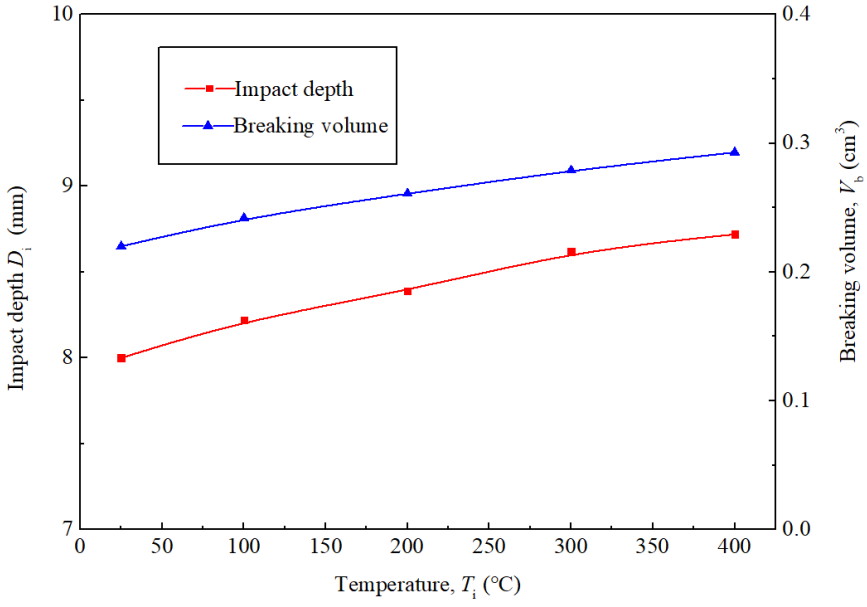

Fig. 8. Temperature effect on the impact depth and depth

4. Conclusions

Establishment and confirmation of the breaking mechanism and optimal parameters of a particle jet for rocks

and other materials to be broken is extremely important. Therefore, the hot dry rock were impacted and broken by a particle jet under various parameters (such as velocity, diameter, concentration, confining presuure, and temperature) both by simulation. The results of this investigation are summarized as follows:

The rebound effect of particles constitutes an important factor in the crater diameter determination during a particle jet impact. The maximum value of the 1st maximum principal stress was 23.1 MPa, which was quite higher than the tensile strength of the rock (marble); therefore, the rock could easily be broken. The higher values of the 1st maximum principal stress were distributed on the surface areas of the crater during the impact progress.

The impact depth and breaking volume increased as the jet inlet velocity increased. The energy increase of particles was the main factor that influenced the rock breaking volume changes. Both the impact depth and breaking volume increased as the particle diameter increased. When the particle diameter exceeded 1.0 mm, the breaking volume began to increase rapidly. The breaking volume of a particle water jet strongly depended on the particle diameter.

Both the impact depth and breaking volume increased as the particle concentration increased. When the particle concentration was below a critical concentration (3%), the impact depth and breaking volume increased rapidly with the increase in the concentration. Moreover, when the particle concentration was >3%, the impact depth and breaking volume increased slowly owing to the interference caused by the collisions between the incident and rebound particles. With the increase of confining pressure, the impact depth and breaking volume decrease. While with the increase of temperature, the impact depth and the breaking volume increase.

Notations

Nomenclature

a	volume correction	-
A, B, N, C	material strength parameters for HJC model	-
C_b	normalization constant	-
C_e	mixing efficiency coefficient	-
C_p	particle volume concentrations	%
C_{MG}	$u_s - u_p$ curve intercept	m/s
D	space dimensionality	-
d_n	nozzle diameter	cm
D	damage ratio	-
D_i	impact depth	mm
E	internal energy per unit volume	-
E_p	elasticity modulus of particles	
h	SPH particle smooth length	-
K_{jet}	waterjet particle kinetic energy	J
m_g	gas mass flow rate	Kg/s
m_p	particle mass flow rate	Kg/s
m_w	water mass flow rate	Kg/s
P_c	confining pressure	MPa
P_w	nozzle pressure	MPa
P_{MG}	pressure	MPa
P^*	dimensionless hydrostatic pressure	-
Q_w	water flow rate	L/s
S_1, S_2, and S_3	$u_s - u_p$ curve slope coefficient	-

v_p	particle inlet velocity	m/s
v_w	jet inlet velocity	m/s
V_b	rock breaking volume	cm^3
T_i	temperature	℃
Greek letters		
γ_0	MIE-GRUNEISEN constant	-
$\bar{\dot{\varepsilon}}^*$	strain rate with a dimension of 1	-
ρ_0	Density	g/cm^3
ρ_p	particle density	g/cm^3
ρ_w	water density	g/cm^3
σ^*	equivalent stress pressure	-
υ_p	Poisson's ratio of particles	
Ω	support domain of the point x	-

Acknowledgements

The authors are pleased to acknowledge the financial support from the National Natural Science Foundation of China (No. 52204022), Major Scientific and Technological Project of CNPC (2022ZG06), Natural Science Foundation of Shandong Province (ZR2022ME152), National Key Research and Development Program of China (2021YFE0111400), Fundamental Research Funds for the Central Universities (19CX02063A), Science and Technology Plan of Dongying City (2021ZD49).

References

[1] A, W, Momber, R. Kovacevic, Deformation and fracture of rocks loaded with spherical indenters, Int. J. Fracture 125 (2004) 206–279.

[2] A. W. Momber, A refined model for solid particle rock erosion, Rock Mech. Rock Eng. 49 (2016) 464–475.

[3] J. N.Sahu, C. Sasikumar, Room temperature Case Carburizing of a Ni–Cr–Mo Steel Through Shot Peening/Blasting Techniques, T. Indian I. Metals 68 (2015) 227–233.

[4] E. M. Szesz, B. L. Pereira, N. K. Kuromoto, et al., Electrochemical and morphological analyses on the titanium surface modified by shot blasting and anodic oxidation processe, Thin. Solid Films 528 (2013) 163–166.

[5] G. A. Tibbtitts, G. G. Galloway, Particle drilling alters standard rock-cutting approach, World Oil 229 (2008) 37–44.

[6] G. A Tibbtitts, G.G. Galloway, J. B. Terry, Impactor excavation system having a drill bit discharging in a cross over pattern, US：8845279B2 2013-7-16.

[7] G. G.Galloway, Shot blocking using drilling mud, US：8342256B2 2013-01-01.

[8] J. Zhao, L. X. Han, Y. J. Xu, et al., A theoretical study and field test of particle impact drilling technology [J]. Natural Gas Industry 34 (2014) 102–107.

[9] A. W. Momber, Wear of rocks by water flow, Int. J. Rock Mech. Min. 41 (2004) 51–68.

[10] J. Zeng, T. J. Kim, A erosion model of polycrystalline ceramics in abrasive waterjet cutting, Wear 193 (1996) 207–217.

[11] G. S. Li, Z.W. Huang, J. L. Niu, et al. The Productivity-Enhancing Technique of Deep Penetrating Perforation with a High-Pressure Water Jet. Pet. Sci. Technol. 25 (2007) 289-297.

[12] C. K. Huang, S. Chinvelli, P.Minev, et al. A comprehensive phenomenological model for erosion of materials in jet flow. Powder Technol. 187 (2008) 273–279.

[13] I. Finnie, Erosion of surfaces by solid particles, Wear 3 (1960) 87–103.

[14] J. Wang, D. M. Guo, A predictive depth of penetration model for abrasive water jet cutting of polymer matrix composites, J. Mater. Process. Tech. 121 (2002) 390–394.

[15] Z. Lin, H. G. Xu, Experimental study of particle erosion in a cavity with a height difference between its walls, Powder Technol. 286 (2015) 378–384.

[16] R. E. Vieira, A. Mansouri, B. S. Mclaury, et al., Experimental and computational study of erosion in elbows due to sand particles in air flow. Powder Technol. 288 (2016) 339–353.

[17] O. Tae-Min, C.Gye-Chun, Characterization of effective parameters in abrasive water jet rock cutting, Rock Mech. Rock Eng. 47 (2014) 745–756.

[18] Y. Y. Lu, J. R. Tang, Z. L. Ge, et al., Hard rock drilling technique with abrasive water jet assistance. Int. J. Rock Mech. Min. 60 (2013) 47–56.

[19] F. Mohammadi, J. L. Luo, B. T. Lu, et al., Single particle impingement current transients for prediction of erosion-enhanced corrosion on 304 stainless steel, Corros. Sci. 52 (2010) 2331–2340.

[20] A. W. Momber, The kinetic energy of wear particles generated by abrasive–water-jet erosion, J. Mater. Process. Tech. 83 (1998) 121–126.

[21] A. Yabuki, M. Matsumura, Theoretical equation of the critical impact velocity in solid particles impact erosion, Wear 233 (1999) 476–483.

[22] C. Narayanan, R. Balz, A.Weiss, et al., Modelling of abrasive particle energy in water jet machining, J. Mater. Process. Tech. 213 (2013) 2201–2210.

[23] S. Paul, A. M. Hoogstrate, C. A. Luttervelt, et al., Analytical modelling of the total depth of cut in the abrasive water jet machining of polycrystalline brittle material. J. Mater. Process. Tech. 73 (1998) 216–212.

[24] M. B. Wang, R. H. Wang, W. Q. Chen, Numerical simulation study of rock breaking mechanism and process under abrasive water jet, Petro. Drill Tech. 37 (2009) 34–38.

[25] C. Y. Kuang, Z. P. Zhu, H. J. Jiang, et al., The experimental study and numerical simulation of single particle impacting rock, Acta. Petrolei. Sinica. 33 (2012) 1059–1063.

[26] K. H. Yu, D. Tafti. Impact model for micrometer-sized sand particles. Powder Technol. 294(2016) 11-12.

[27] Y. J. Xu, H, X. Zhao, W. L. Sun, et al., Numerical analysis on rock breaking effect of steel particles impact rock. J. China Univ. Petrol. 33 (2009) 68–69.

[28] K. S. Wu, J. F. Gu, C. Y. Kuang, et al., Comment on particle impact drilling technology, J. Southwest Petrol. 30 (2008) 142–146.

[29] M. Petrica, E. Badisch, T.Peinsitt, Abrasive wear mechanisms and their relation to rock properties, Wear, 308 (2013) 86–94.

[30] A. W. Momber, Effects of target material properties on solid particle erosion of geomaterials at different impingement velocities, Wear 319, (2015) 69–83.

[31] A. W. Momber, Erosion of schist due to solid particle impingement, Rock Mech. Rock Eng. 46 (2013) 849–857.

[32] V. Hadavi, M. Papini, Numerical modeling of particle embedment during solid particle erosion of ductile materials, Wear 342 (2015) 310–321.

[33] C. Goodin, J. D. Priddy, Comparison of SPH simulations and cone index tests for cohesive soils, J. Terra. Mechanics 66 (2016) 49–57.

[34] D. Meric, H.Gedikli. Energy absorption behavior of tailor-welded tapered tubes under axial impact loading using coupled FEM/SPH method. Thin Wall Struct. 104 (2016) 17–33.

[35] L. Aktay, A. F.Johnson, A. K. Toksoy, et al., Modeling the progressive axial crushing of foam-filled aluminum tubes using smooth particle hydrodynamics and coupled finite element model/smooth particle hydrodynamics, Mater. Design 29 (2008) 569–575.

[36] M. Bielawski W. Beres, FE modelling of surface stresses in erosion-resistant coatings under single particle impact, Wear. 262 (2007) 167–175.

[37] Z. H. Sun, Dynamics response analysis of penetration based on FE-SPH adaptive coupling method, The Hunan Univ. Press, Changsha, China, 2012.

[38] Q. X. Xu, Study of some impact dynamics problems based on smoothed particle hydrodynamics method, The Shanghai Jiao Tong Univ. Press, Shanghai, China, 2009.

[39] X. D. Lu, Y. H. Huang, Y. J. Tang, et al., Simulation process of abrasive impacting a workpiece surface based on SPH method, J.

Vib. Shock 32 (2013) 169–174.

[40] O. Heuze, General form of the Mie-Gruneisen equation of state, C. R. Mecanique 340 (2012) 679–687.

[41] W. Zhang, D. A. Hu, X. Han, Simulation on projectile penetration into moving ceramic/metal composite armor using SPH method, Chin. J. Solid Mech. 31 (2010) 70–75.

[42] A. P. Chernyshev, The Mie-Gr¨uneisen equation of state for metal nanoparticles, Eur. Phys. J. E.79 (2011) 321–325.

[43] X. D. Lin, Y. Y. Lu, J. R. Tang, et al., Numerical simulation of abrasive water jet breaking rock with SPH-FEM coupling algorithm, J. Vib. Shock 33 (2014) 170-175.

[44] R. Q. Zhang, Y. Q. Ding, H. W. Tang, et al., The failure strength parameter of HJC and RHT concrete constitutive models, Chin. J. High Pressure Phys. 25 (2011) 15–21.

[45] X. Z. Kong, Q. Fang, H. Wu, et al., Numerical predictions of cratering and scabbing in concrete slabs subjected to projectile impact using a modified version of HJC material model, Int. J. Impact Eng. 95 (2016) 61–71.

[46] X. T. Wu, Y. Li, H. P. Li, et al., Research on the material constants of HJC dynamic constitutive model for concrete, Chin. J. Appl. Mech. 25 (2011) 340–345.

[47] M. Polanco-Loria, O. S. Hopperstad, T. Borvik, Numerical predictions of ballistic limits for concrete slabs using a modified version of the HJC concrete model, Int. J. Impact Eng. 35 (2008) 290–303.

[48] A.W. Momber , 1, 2, R. Kovacevic Test parameter analysis in abrasive water jet cutting of rocklike materials Int. J. Rock Mech. Min. 34 (1997) 17-25.

[49] X. H. Zhu, L. He, W. J. Liu, et al., Research on particle jet and its auxiliary drill tooth breaking law, J. Southwest Petrol. Univ. https://kns.cnki.net/kcms/detail/51.1718.te.20201231.0958.002.html (2020) 1-11.

[50] M. T. Benchaita, P. Griffith, E. Rabinnowic, Erosion of metallic plate by solid particle entrained in a liquid jet, J. Engine Ind. 105 (1983) 215–222.

[51] H. M. Clark, R. B. Hartwich, A re-examination of the ‘particle size effect’ in slurry erosion, Wear 248 (2001) 147–161.

[52] V. B. Nguyen, Q. B. Nguyen, Y. W. Zhang, et al., Effect of particle size on erosion characteristics. Wear, 348 (2016) 126-137.

[53] F. S. Ren, T. C. Fang, X. Z. Cheng, Study on rock damage and failure depth under particle water-jet coupling impact. Int. J. Impact Eng. 139 (2020) 103504.

[54] D. R. Andrews, N. Horsfield, Particle collisions in the vicinity of an eroding surface, Journal of Physics D: Applied Physics 16 (1983) 525-538.

[55] T. Burzynski, M. Papini, Analytical models of the interference between incident and rebounding particles within an abrasive jet: Comparison with computer simulation, Wear 263 (2007) 1593-1601.

[56] M. Papini, D. Ciampini, T. Krajac, et.al., Computer modelling of interference effects in erosion testing: effect of plume shape, Wear 255 (2003) 85-97.

[57] D. Ciampini, J. K. Spelt, M. Papini, Simulation of interference effects in particle streams following impact with a flat surface. Part I. Theory and analysis, Wear 254 (2003) 237–249.

[58] J. C. Song, Z. J. Wang, Y. Li, et al., Research on granite cutting and breaking test under conditions of high temperature and high pressure, Chi. J. Rock Mech. Eng. 28 (2009) 1422–1438.